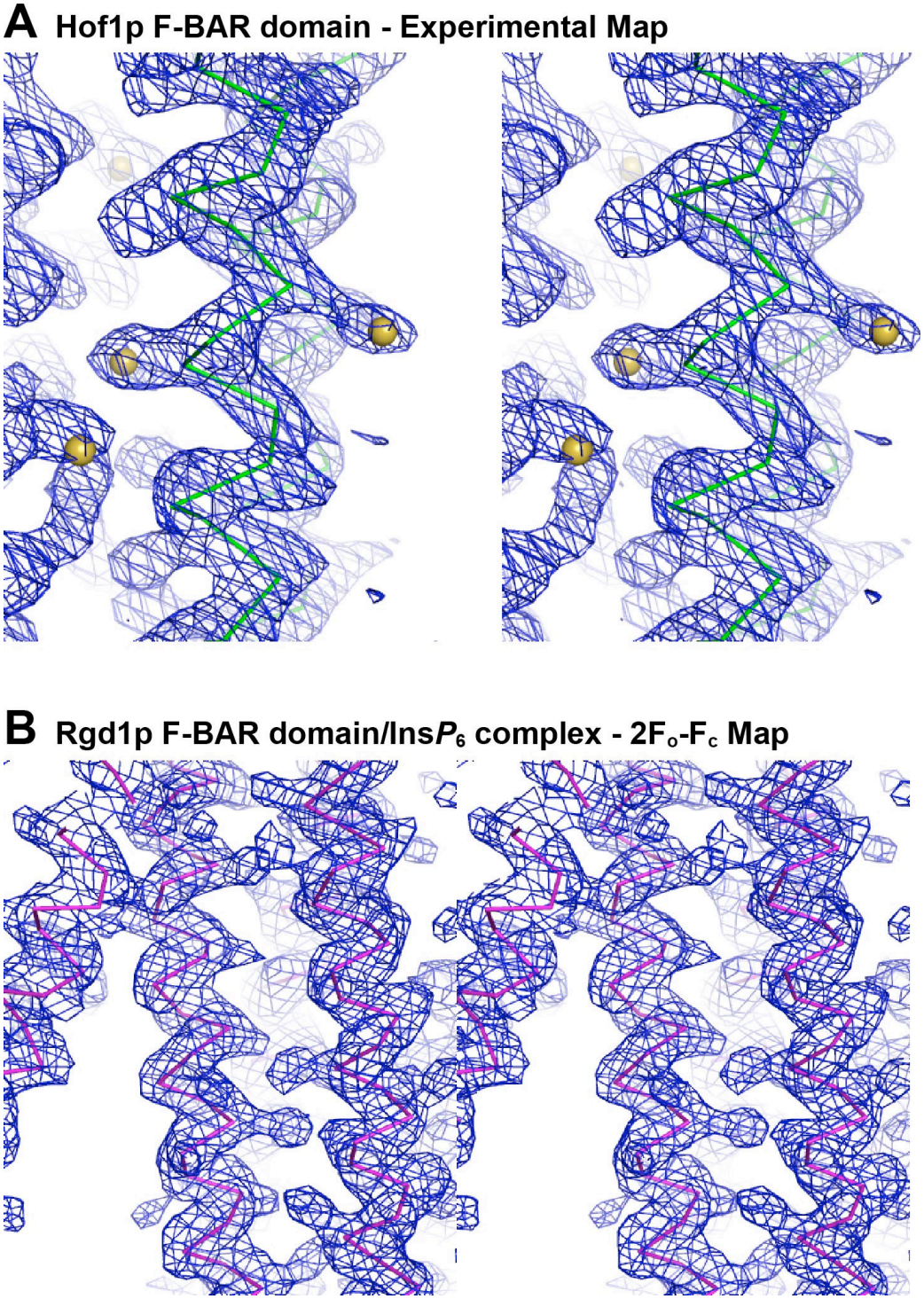

Figure S1, related to Table 1.
Representative electron density for Hof1p and Rgd1p F-BAR structures.
(**A**) Experimental Se-MAD density map for Hof1p F-BAR, generated, contoured at 1.5σ. Se atoms are shown as gold spheres, and a representative Hof1p α-helix is shown as a green ribbon. (**B**) $2F_o$-Fc map contoured at 1σ for the Rgd1p F-BAR structures, solved using molecular replacement.

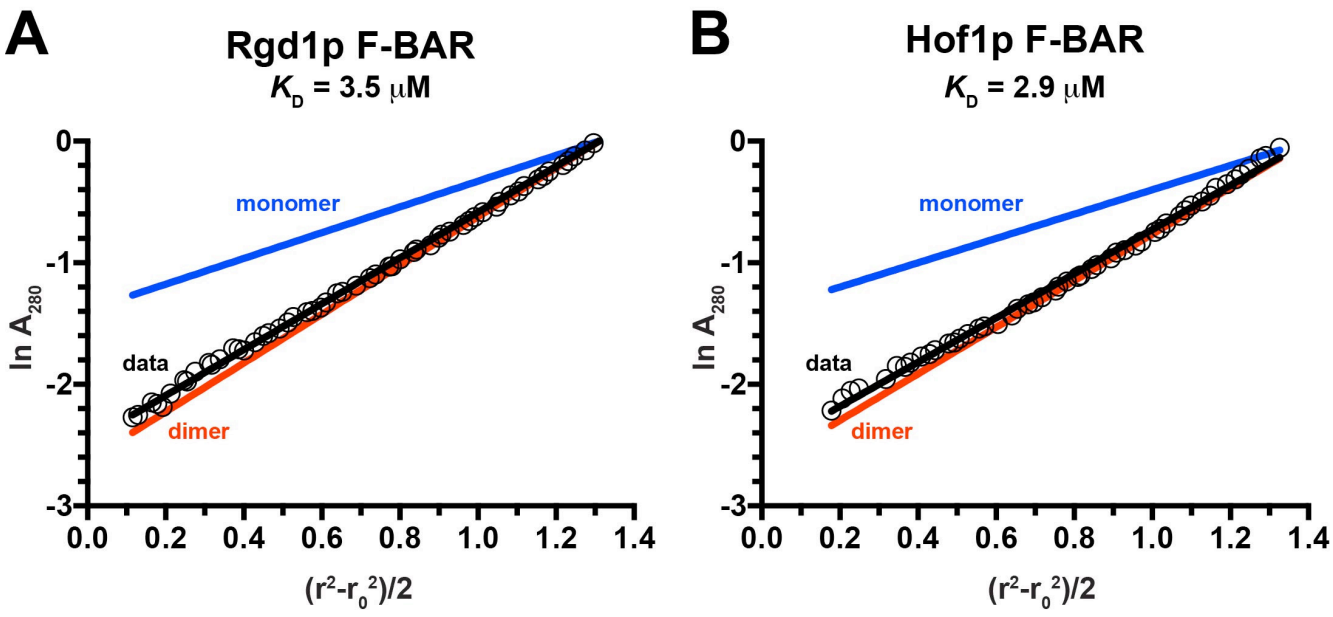

Figure S2, related to Figure 3.
***S. cerevisiae* F-BAR domains are dimeric in solution.**
Dimerization of the F-BAR domains from (**A**) Rgd1p (aa 24-333aa), and (**B**) Hof1p (aa 1-300) were assessed by sedimentation equilibrium analytical ultracentrifugation. Experiments were performed at 15 μM, 23 μM and 30 μM for Rgd1p F-BAR and 9 μM, 13 μM and 18 μM for Hof1p F-BAR, at speeds of 6,000, 9,000, 12,000 and 15,000 rpm in each case (at 25˚C). Representative data from 15,000 rpm experiments are shown (open black circles), revealing that the protein is predominantly dimeric. Data are plotted as the natural logarithm of the absorbance at 280 nm (A_{280}) versus $(r^2-r_0^2)/2$, where r is the radial distance of the sample and r_0 is the radial distance of the meniscus. For a single ideal species, the slope of the line in this representation is proportional to molecular weight of the species. Expected data for ideal monomeric and dimeric F-BAR domains are drawn in blue and red, respectively, and the experimental data closely approximates the result expected for a dimer. Global fitting of all data at three concentrations and four speeds yielded the K_D values shown in the figure (~3 μM) for F-BAR domain dimerization in each case. Data were analyzed using Sedfit and Sedphat (http://analyticalultracentrifugation.com).

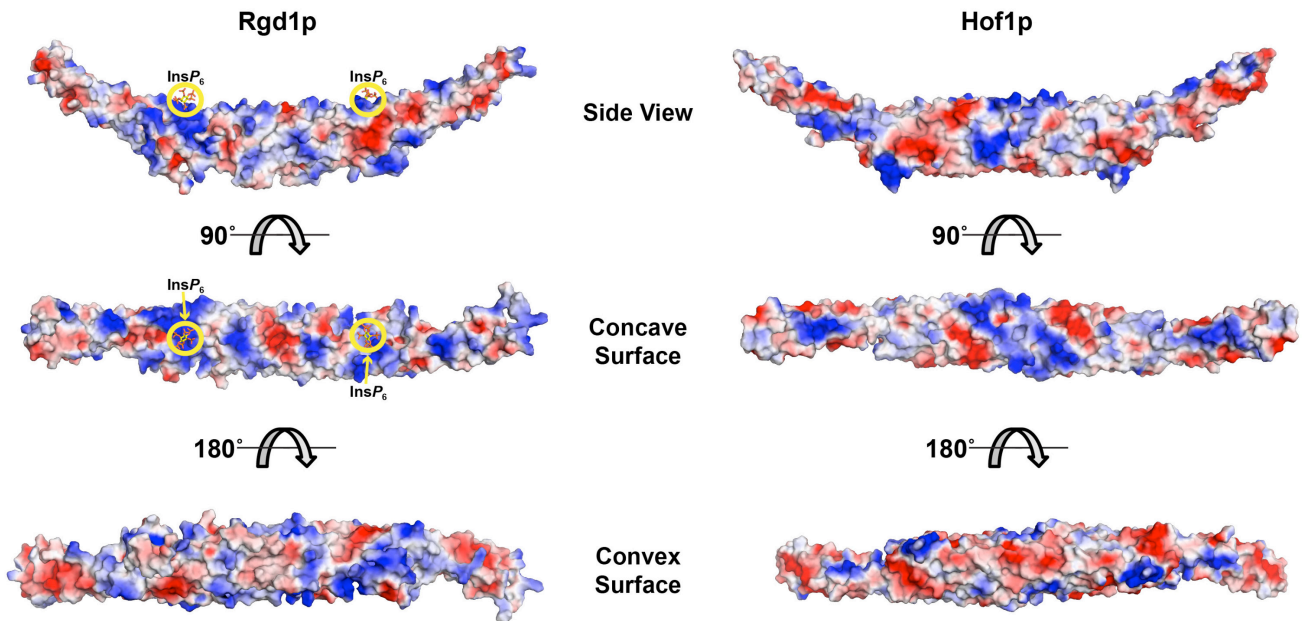

Figure S3, related to Figure 3.
Electrostatic surface potential of Rgd1p and Hof1p F-BAR domains.
The F-BAR domains from Rgd1p (left) and Hof1p (right) are shown in the same set of orientations used for Figure 3, but in surface representation, colored according to electrostatic surface potential (blue, positive; red, negative). The upper view is a side view in each case, showing the straight rounded-bracket shape. The middle view represents a view into the concave surface, where membrane is believed to bind. The InsP_6 molecules are found bound to this surface in the Rgd1p F-BAR dimer. The bottom view is a view directed at the convex surface.

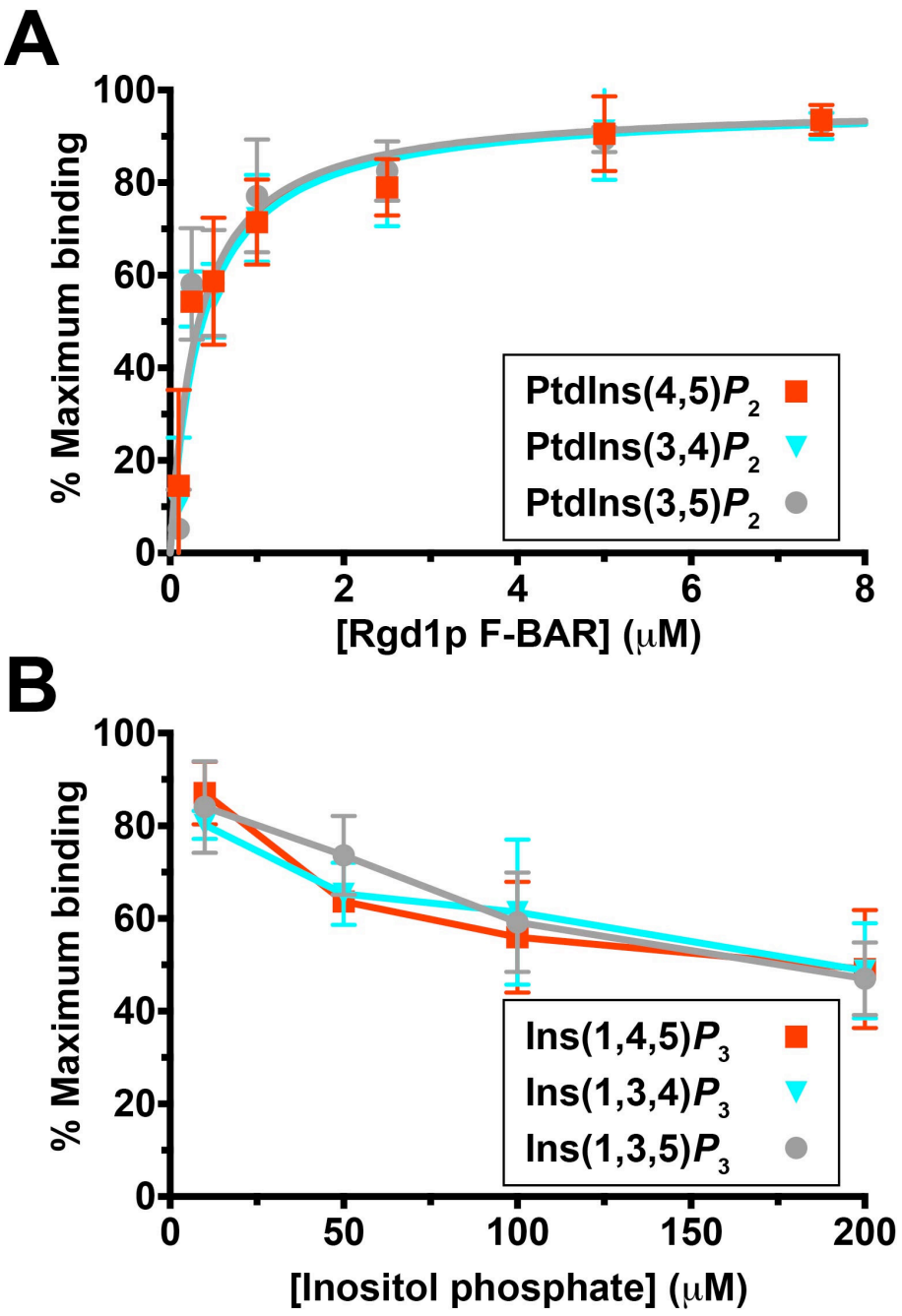

Figure S4, related to Figure 4.
Absence of stereospecificity in phosphoinositide recognition by Rgd1p F-BAR.
(**A**) Surface plasmon resonance (SPR) studies of Rgd1p F-BAR binding to DOPC membranes containing 10% (mole/mole) PtdIns(4,5)P_2 (red), PtdIns(3,4)P_2 (cyan) or PtdIns(3,5)P_2 (grey). SPR binding signal is plotted as percentage of the maximal binding signal (B_{max}) obtained at saturation against protein concentration. Data are shown as mean ± standard deviation for at least 3 independent experiments.
(**B**) Competition studies showing that three different InsP_3 isomers, Ins(1,4,5)P_3, Ins(1,3,4)P_3 and Ins(1,3,5)P_3 are equally potent in displacing the Rgd1p F-BAR domain (at 5μM) from a sensorchip surface bearing vesicles with 10% PtdIns(4,5)P_2 (mole/mole) in a DOPC background. Data are shown as mean ± standard deviation for at least 3 independent experiments.

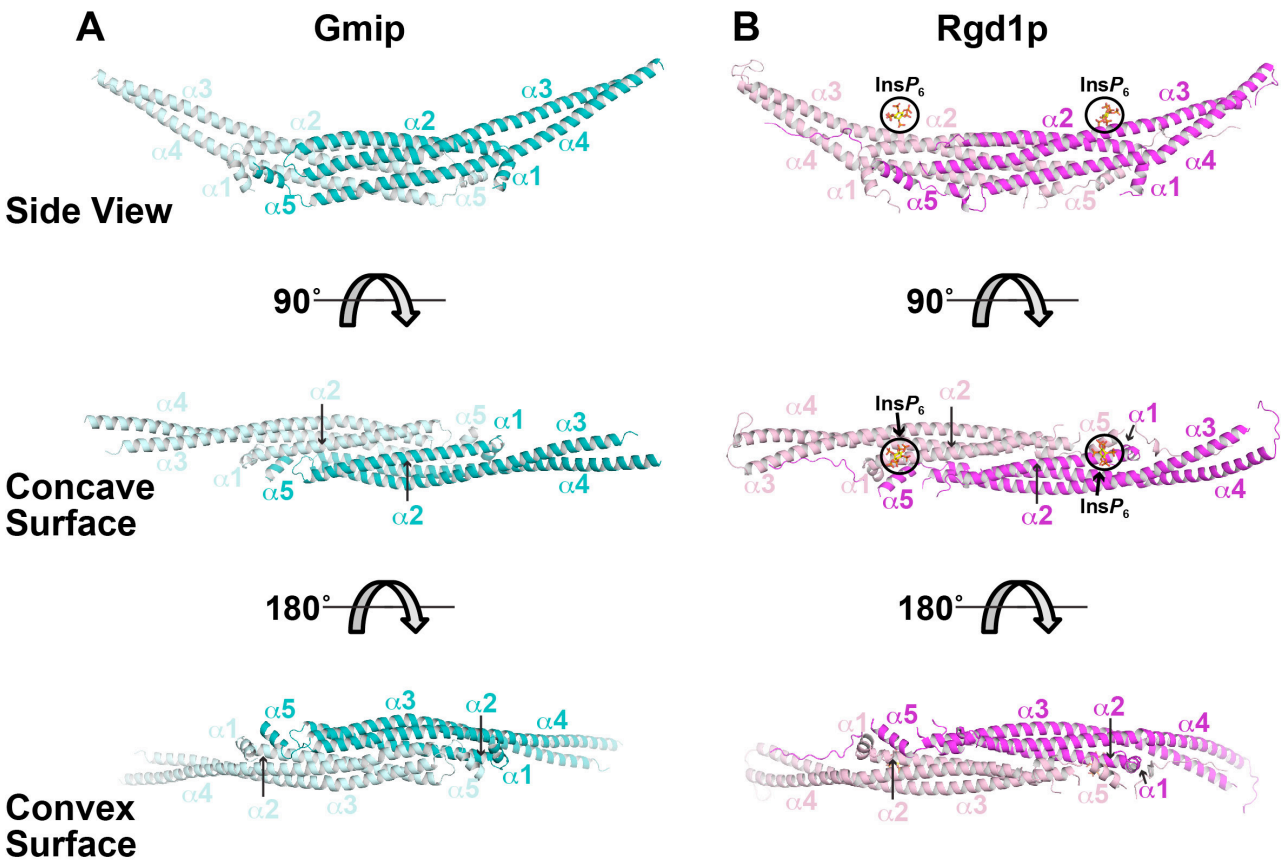

Figure S5, related to Figure 6.
Comparison of Gmip and Rgd1p F-BAR domain structures.
The F-BAR domain structures from (**A**) Gmip (PDB entry 3QWE) and (**B**) Rgd1p are shown in the same orientations used for Figure 3, showing that, in addition to preserving the inositol phosphate binding site, the Gmip F-BAR domain shares the rounded bracket shape seen in Rgd1p and Hof1p F-BARs.